

The Spectral Decay Parameter Kappa in Northeastern Sonora, Mexico

by Avelina I. Fernández,* Raúl R. Castro, and Carlos I. Huerta

Abstract We calculated the spectral decay parameter (κ) in the southern Basin and Range province, using records from earthquakes located near the Pitáycachi fault. We found that for a given distance and recording site the values of κ vary considerably, possibly as a result of the lateral heterogeneity of the crust. Individual values of κ do not show a clear trend with magnitude, nor with the average values of κ . The average values of κ tend to increase with distance up to about 70–80 km and then to decrease between 80 and 100 km, suggesting higher S -wave attenuation at shallow depths and lower attenuation for deeper paths. We analyzed the possible dependence of κ on earthquake size by determining empirical curves that describe the behavior of κ with distance and magnitude. Our results indicate that κ is independent of earthquake size within the magnitude range ($M < 3.5$) of the events analyzed. The nonparametric curves also provided site-specific estimates of κ near the surface (κ_0) for the stations and groups of stations analyzed. We found that the average κ_0 value of 0.04 sec in northeastern Sonora is similar to values of κ_0 reported in other regions. We conclude that κ_0 depends not only on the rock type but also on the degree of fracturing and erosion of the rocks near the recording site.

Introduction

The spectral decay parameter κ (Anderson and Hough, 1984) is useful for describing the high-frequency ground-motion spectra and has been used extensively to simulate ground-motion acceleration from moderate and large earthquakes (Rovelli *et al.*, 1988; Beresnev and Atkinson, 1997; Castro *et al.*, 2001; Bindi *et al.*, 2004; among others). Anderson and Hough (1984) defined κ to describe the shape of the high-frequency spectra as $A(f) \sim \exp(-\pi\kappa f)$. In this model the high-frequency fall-off results from attenuation along the propagation path and near the surface. However, recent studies have proposed a different origin of the high-frequency spectral decay. For instance, Petukhin and Irikura (2000) reported that the spectral fall-off has a source origin, and Tsai and Chen (2000) reported that it is a combination of near-surface attenuation and source effect. These studies agree with the model of Papageorgiou and Aki (1983) that proposes the high-frequency fall-off as a source effect. More recently, Purvance and Anderson (2003) found that in the Guerrero subduction zone κ results from two similar contributing components. One component is related with the recording site (κ_{site}) and corresponds to the average value of κ for each station. The other component is related with the events recorded (κ_{event}) and is estimated as the average value of κ for each event. It was found that κ_{event} is on aver-

age 4.5 msec less in normal faulting earthquakes than in thrusting events.

In this article, we estimated κ using earthquakes that occurred in the southern Basin and Range province, where the extensional regime characteristic of this region generates normal faulting earthquakes. We also analyze if the size of the events affects the observed values of κ .

The northeastern region of Sonora, Mexico, is characterized by the existence of a north–south striking normal fault system that is distributed on the western limit of the Sierra Madre Occidental (Fig. 1). These faults are responsible for the occurrence of a major earthquake in this region on 3 May 1887, with moment magnitude 7.5. This earthquake broke three neighboring segments, known as Oates, Teras, and Pitáycachi, of the fault system that generated a rupture trace of more than 100 km in length (Suter and Contreras, 2002).

To study the seismicity of northeastern Sonora, Castro *et al.* (2002) installed (in 2002) the Seismic Network of Northeastern Sonora (Red Sísmica del Noreste de Sonora [RESNES]), which has registered numerous earthquakes of different magnitudes ($M < 4$), demonstrating that there is recent seismic activity in this region.

Previous attenuation studies in northeastern Sonora have been made by Condori (2006) and Castro *et al.* (2008). These authors made estimates of the quality factor Q using body waves from local and regional earthquakes recorded by RESNES between 2003 and 2004. They found that in the region of the 1887 rupture, $Q_P = 20.8f^{1.1}$ and $Q_S = 83.8f^{0.9}$

*Also at Centro Nacional de Investigaciones Sismológicas (CENAI), Calle 17 No. 61 e/ 4 y 6 Vista Alegre, 90400 Santiago de Cuba, Cuba, idalmis@cicese.mx.

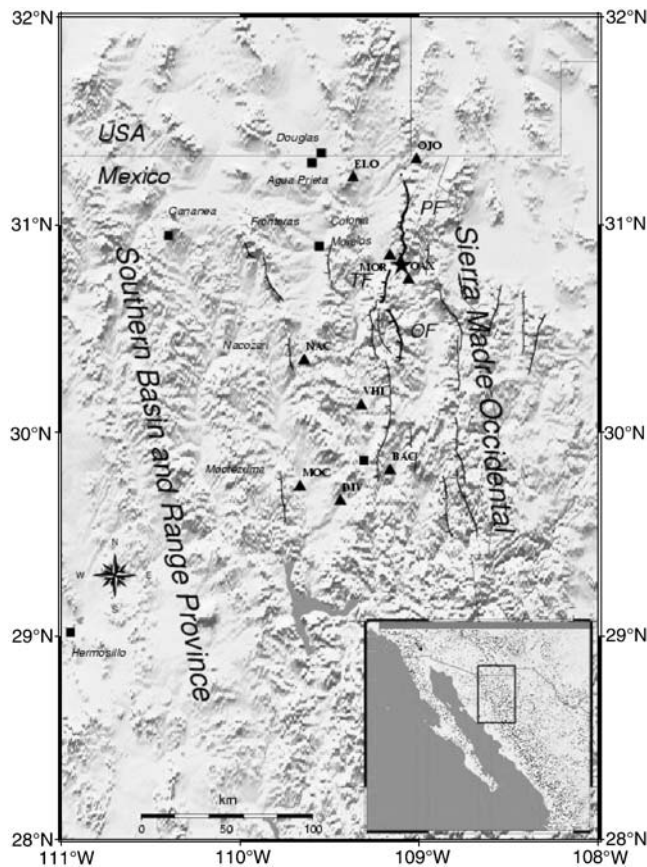


Figure 1. Map showing the distribution of the stations (triangles); the fault segments that ruptured during the 1887 earthquake (PF, Pitáycachi; TF, Teras; and OF, Oates); and the main population centers (squares). The star indicates the location of the epicenter of the 3 May 1887 earthquake.

in the 0.63–63.1 Hz frequency band. The reported $Q_S/Q_P > 1.9$ ratio suggests that scattering may be an important mechanism controlling the observed decay of spectral amplitudes with distance.

In the present study, we analyze the high-frequency spectral-amplitude decay of local earthquakes by determining the spectral decay parameter κ . Because this parameter includes both common source-station path attenuation and near-surface attenuation under the recording stations (Anderson, 1991), κ is a very useful parameter for modeling the acceleration spectra at high frequencies (Anderson and Hough, 1984).

We analyze the attenuation of northeastern Sonora, Mexico, estimating κ at different sites and source-station distances, and we also study the possible dependence of κ with earthquake size. Then, we separate the distance and near-surface effects from κ , calculating empirical curves that describe the behavior of the spectral decay parameter κ with the distance r and magnitude. These curves permit the estimation of κ near the surface (κ_0) for every analyzed station and for groups of stations with similar lithology characteristics by extrapolating the curves at $r = 0$.

Data

RESNES (Fig. 1) was installed with the aim of documenting regional seismicity associated with the faults that ruptured during the occurrence of the 1887 earthquake. This network consists of nine digital stations that record three components of ground acceleration (north–south, east–west, and vertical) and the vertical component of ground velocity (Castro *et al.*, 2002). In this article, we consider only the horizontal components of ground-motion acceleration. Figure 2 shows an example of an accelerogram recorded at station Ojos Calientes (OJO) from a local earthquake located about 26 km from that station. The vertical component of ground velocity is also displayed in Figure 2.

According to the physiographic features reported for the state of Sonora by the Mexican National Institute of Statistics, Geography and Information (2006) (Instituto Nacional de Estadística y Geografía [INEGI]), the stations of RESNES are located within the two physiographic provinces of the region of Sonora: the Sierra Madre Occidental (SMO) and the southern Basin and Range province (SBR). The SMO consists of a large igneous structure oriented northwest–southeast, with many normal faults that have formed tectonic trenches and pillars that resemble the shape of a vast plateau. Its western flank is more rugged than the eastern due to faulting. Precambrian in this province is represented by metamorphic rocks, located at the base of the mountains, and Paleozoic and Mesozoic formations are represented by limestone and detrital rocks, some with various degrees of metamorphism. The SBR province covers the western side of our region of study and contains Paleozoic limestone, detrital calcareous rocks, and intrusive bodies of acid composition

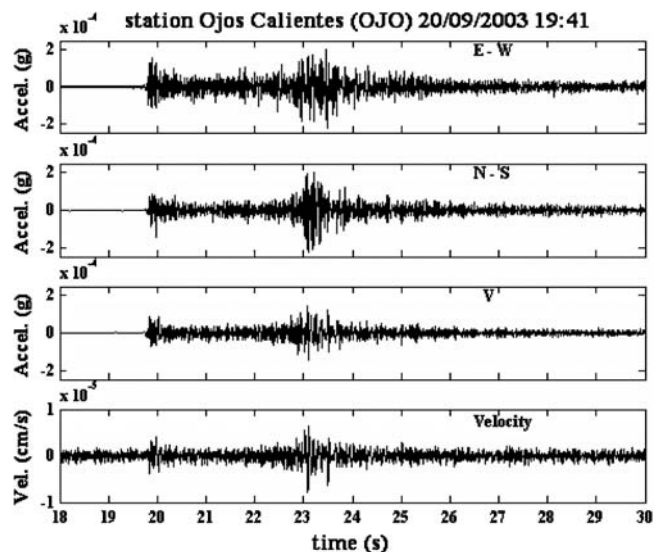


Figure 2. The first three frames (from the top) are the east–west, the north–south, and the vertical components of ground acceleration recorded at station Ojos Calientes (OJO) from a local earthquake located about 26 km from the station. The bottom frame corresponds to the vertical component of ground velocity at the same station.

from Mesozoic time. In the SBR province, acidic and basic volcanic rocks from the Cenozoic and conglomerates from the Tertiary form hills with gentle slopes. Quaternary soils are partially scarce and mostly located in lower areas.

Stations OJO, ELO, and NAC, displayed in Figure 1, are on extruded acid to intermediate igneous rocks. Station DIV is on extruded acid igneous rocks of the Cretaceous. Stations OAX, MOR, VHI, MOC, and BAC are on continental deposits (Tertiary conglomerates).

We analyzed 1183 records of ground acceleration (575 north–south and 608 east–west component) registered by nine stations of the RESNES array. The number of earthquakes per station analyzed varies between 31 and 150, and the magnitudes range between 0.5 and 3.5. We selected records with high signal-to-noise ratio and clear S -wave arrivals, covering a range of distances between 0 and 100 km. At this distance range the seismic records are mainly influenced by the near-surface structure of the crust because most source-station ray paths are confined to the crust.

Method

At high frequencies, the shape of the acceleration spectrum can be described by the following equation (Anderson and Hough, 1984):

$$A(f) = A_0 e^{-\pi\kappa f}, \quad f > f_E. \quad (1)$$

A_0 depends on source properties, epicentral distance, and other path related factors; f_E is the frequency above which the spectral shape has an exponential decay; and κ is the spectral decay parameter.

To estimate κ from the selected recordings, the acceleration spectra were calculated finding the fast Fourier transform of a window containing S -wave arrivals. We used a window length that includes the maximum amplitude of the wave and avoids overlapping with other types of waves that arrive after the S wave. The beginning of the window was selected at the time of the first S -wave arrival, and the end of the window selected when 80% of the total energy was reached. Thus, the length of this time window may be different for different events, depending on the magnitude of the earthquake and the hypocentral distance. Small events recorded at short distances tend to have shorter time-window lengths.

The records were previously baseline corrected subtracting the average of all points of the record. The beginning and the end of the time windows were cosine tapered and the spectral amplitudes smoothed at predefined frequencies between 0.4 and 50 Hz with a variable frequency band of $\pm 25\%$ of the central frequency.

To estimate κ we calculated the linear least-squares fit of the observed acceleration spectra in a log-linear space using equation (1) as a reference model. Figure 3 shows the frequency windows used for each station to calculate κ . The dark line corresponds to the average at each station from

all spectra, and the fine lines are examples of observed spectra at different distances between 0 and 100 km. We chose the frequency windows that we considered appropriate at each station based on the average spectrum and the behavior of the high-frequency fall-off of the majority of the observed spectra. The beginning and the end of the windows correspond with the frequencies at which the spectral amplitude starts to decrease exponentially and when the amplitudes stop decreasing due to background noise, respectively. The selection of the lower frequency limit (f_e) is intended to minimize corner frequency contamination. For stations BAC, MOR, and OAX (Fig. 3), the corner frequency of many of the events is below 6 Hz; for this reason we chose $f_e = 6$ Hz. Another justification for the selection of f_e comes from the estimates of Q reported by Castro *et al.* (2008, 2009) in this region that show a weak frequency dependence of Q above 6 Hz. Except for stations MOC and NAC, which seem to have corner frequencies below 2 Hz, for the rest of the stations we selected f_e above 6 Hz. To analyze the distance (r) and site dependence (z) of κ , we used the model proposed by Anderson (1991), in which the values of κ estimated for each station can be represented by a function $\kappa(r, z)$ that describes the distance dependence of κ at a given site z . In this model, the function that describes the distance dependence of κ is assumed to be the same for all sites, and the near-surface attenuation ($\kappa_0(z)$) is assumed to be unique among each site and dependent on the geologic conditions near the recording station.

The mathematical formulation of this model can be written as

$$\kappa(r, z) = \kappa(r) + \kappa_0(z). \quad (2)$$

Although at high frequencies it is usually assumed that the spectral amplitudes are not influenced by the effect of the source, we consider that κ may also depend on the size of the earthquakes, and we included this consideration in equation (2):

$$\kappa(r, M_D, z) = \kappa(r, M_D) + \kappa_0(z). \quad (3)$$

We estimated the duration magnitude (M_D) of the events analyzed using the equation obtained by González and García (1986):

$$M_D = 2.2 \log(T) - 0.85. \quad (4)$$

The duration (T) of the events is measured from the beginning of the first P -wave arrival until the signal-to-noise ratio takes an approximate value of less than 2.

To find the functional dependence of κ with r , M_D , and the near-surface contribution $\kappa_0(z)$, we used a non-parametric approach similar to that proposed by Anderson and Lei (1994). Equation (3) represents a system of

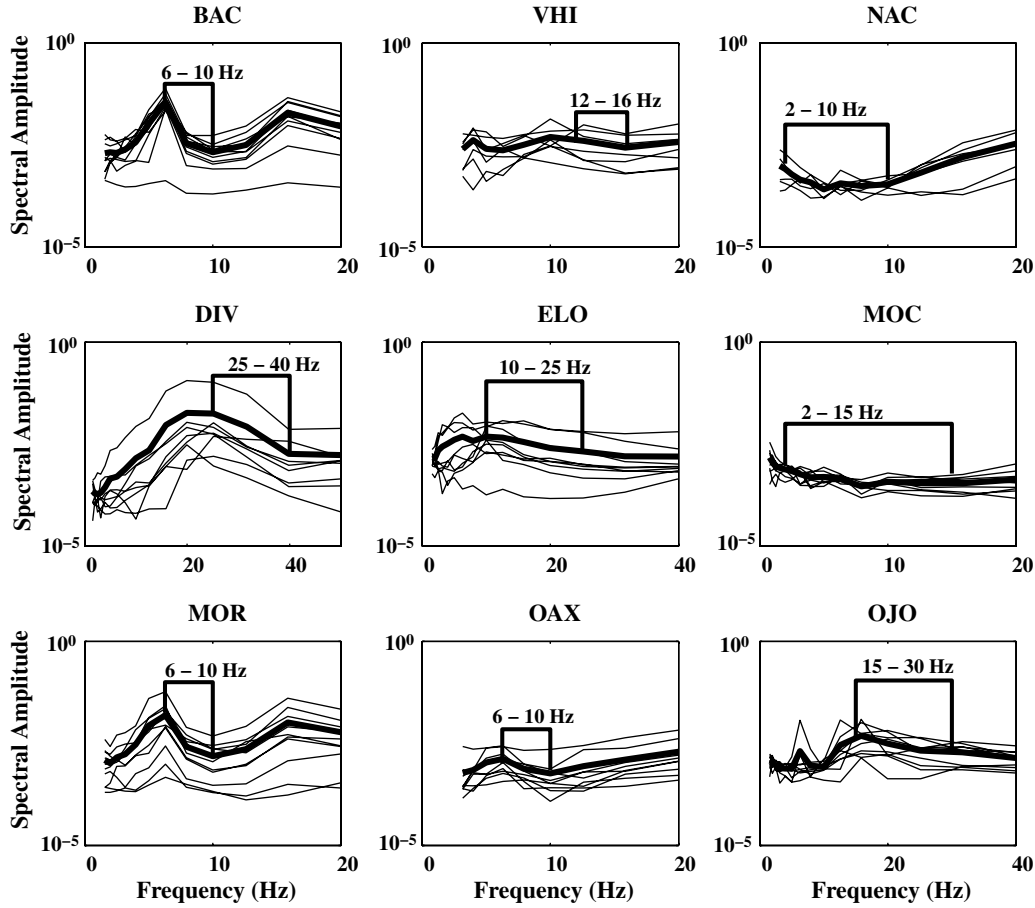


Figure 3. Frequency windows used to estimate κ . The beginning of the window corresponds to the frequency f_e at which the spectral amplitude starts a predominant exponential decrease. The end of the window is the frequency at which the noise interrupts the exponential decay. The dark line corresponds to the average of all spectra at each station, and the fine lines are examples of spectra calculated at different distances in the 0–100 km range.

equations where the left-hand side is the observed estimates of κ at station z from an earthquake at epicentral distance r and magnitude M_D . In matrix form this system of equations can be written as

$$\begin{bmatrix} c_{11}^1 & c_{12}^1 & \dots & c_{ij}^1 \\ c_{11}^2 & c_{12}^2 & \dots & c_{ij}^2 \\ \vdots & \vdots & \vdots & \vdots \\ c_{11}^N & c_{12}^N & \dots & c_{ij}^N \\ w_{11}^1 & w_{12}^1 & \dots & w_{ij}^1 \\ \vdots & \vdots & \vdots & \vdots \\ w_{11}^M & w_{12}^M & \dots & w_{ij}^M \end{bmatrix} \begin{bmatrix} K_{11} \\ K_{12} \\ \vdots \\ K_{ij} \\ K_{01} \\ K_{02} \\ \vdots \\ K_{0Z} \end{bmatrix} = \begin{bmatrix} D^1 \\ D^2 \\ \vdots \\ D^N \\ 0 \\ 0 \\ \vdots \\ 0 \end{bmatrix}. \quad (5)$$

For a distance r in the interval $\mathbf{R}_l \leq r \leq \mathbf{R}_{l+1}$ and magnitude M_D in the interval $\mathbf{M}_k \leq M_D \leq \mathbf{M}_{k+1}$, where \mathbf{R} is a given distance vector with J elements and \mathbf{M} is a given magnitude vector with I elements:

$$\begin{aligned} C_{i-lj-1}^N &= (\mathbf{M}_{k+1} - \mathbf{M}) / (\mathbf{M}_{k+1} - \mathbf{M}_k) \\ &\quad \times (\mathbf{R}_{l+1} - r) / (\mathbf{R}_{l+1} - \mathbf{R}_l), \\ C_{i-lj}^N &= (\mathbf{M}_{k+1} - \mathbf{M}) / (\mathbf{M}_{k+1} - \mathbf{M}_k) \\ &\quad \times (r - \mathbf{R}_l) / (\mathbf{R}_{l+1} - \mathbf{R}_l), \\ C_{ij-1}^N &= (\mathbf{M} - \mathbf{M}_k) / (\mathbf{M}_{k+1} - \mathbf{M}_k) \\ &\quad \times (\mathbf{R}_{l+1} - r) / (\mathbf{R}_{l+1} - \mathbf{R}_l), \\ C_{ij}^N &= (\mathbf{M} - \mathbf{M}_k) / (\mathbf{M}_{k+1} - \mathbf{M}_k) \\ &\quad \times (r - \mathbf{R}_l) / (\mathbf{R}_{l+1} - \mathbf{R}_l). \end{aligned} \quad (6)$$

In equation (5), D^N are the values of κ estimated from the observed acceleration spectra at different distances and event magnitudes from station z ; K_{ij} are discrete values of the unknown function $\kappa(r, M_D)$; κ_{0Z} is the κ_0 value for station z , and N is the number of observations of κ .

We constrained $\kappa(r, M_D, z)$ to be a smooth surface; thus, we incorporated a smoothing constraint that consists of imposing a weighted finite difference approximation for

the first and second derivatives of K_{ij} with respect to the distance. These can be expressed as

$$\begin{aligned} w_1(K_{ij} - K_{i+1j}) &= 0, & i &= 1, 2, \dots, I-1; \\ w_2(K_{ij} - K_{ij+1}) &= 0, & j &= 1, 2, \dots, J-1; \\ w_1(K_{ij} - 2K_{i+1j} + K_{i+2j}) &= 0, & i &= 1, 2, \dots, I-2; \\ w_2(K_{ij} - 2K_{ij+1} + K_{ij+2}) &= 0, & j &= 1, 2, \dots, J-2. \end{aligned} \quad (7)$$

These smoothing constraints are included in the last \mathbf{M} lines of the sensitivity matrix of equation (5), where w_1 and w_2 are the weighting factors for magnitude and distance, respectively, and $\mathbf{M} = I + J - 4$. We tested three different values for the weighting factors w_1 and w_2 , following [Anderson and Lei \(1994\)](#). We used weights of 0.1 for very light smoothing (for the first derivative), 1.0 for an intermediate smoothing (first derivative), and 2.0 for a strong smoothing (for the second derivative). We finally decided to use an intermediate smoothing criteria with $w_1 = w_2 = 1.0$.

The vector \mathbf{R} was selected to take the values of 5, 10, 15, 20, 25, 30, 35, 40, 45, 50, 55, 60, 65, 70, 75, 80, 85, 90, 95,

and 100 km, and the vector \mathbf{M} to take the values of 0.25, 0.5, 0.75, 1.00, 1.25, 1.50, 1.75, 2.00, 2.25, 2.50, 2.75, 3.00, 3.25, 3.50, 3.75, and 4.00. Then, equation (5) was solved using a nonnegative least-squares algorithm.

Results

Figure 4 shows the values of κ estimated by linear least-squares fits of the observed acceleration spectra at stations BAC and MOR for distances between 0 and 100 km. To reduce the scatter due to lateral heterogeneities and other effects not included in the term A_0 of equation (1), we averaged the values of κ at 5 km intervals. The averaged values of κ tend to increase with distance up to about 70–80 km and then to decrease between 80 and 100 km.

Similarly, Figure 5 (top row) shows the values of κ versus magnitude estimated at stations OAX and DIV for events with $M_D < 3.5$, and Figure 5 (bottom row) shows the averaged values of κ at 0.25 magnitude intervals. The individual values of κ (top row of Fig. 5) for the stations shown, and for the other stations as well, do not show a clear trend with M_D , nor with the averaged values of κ .

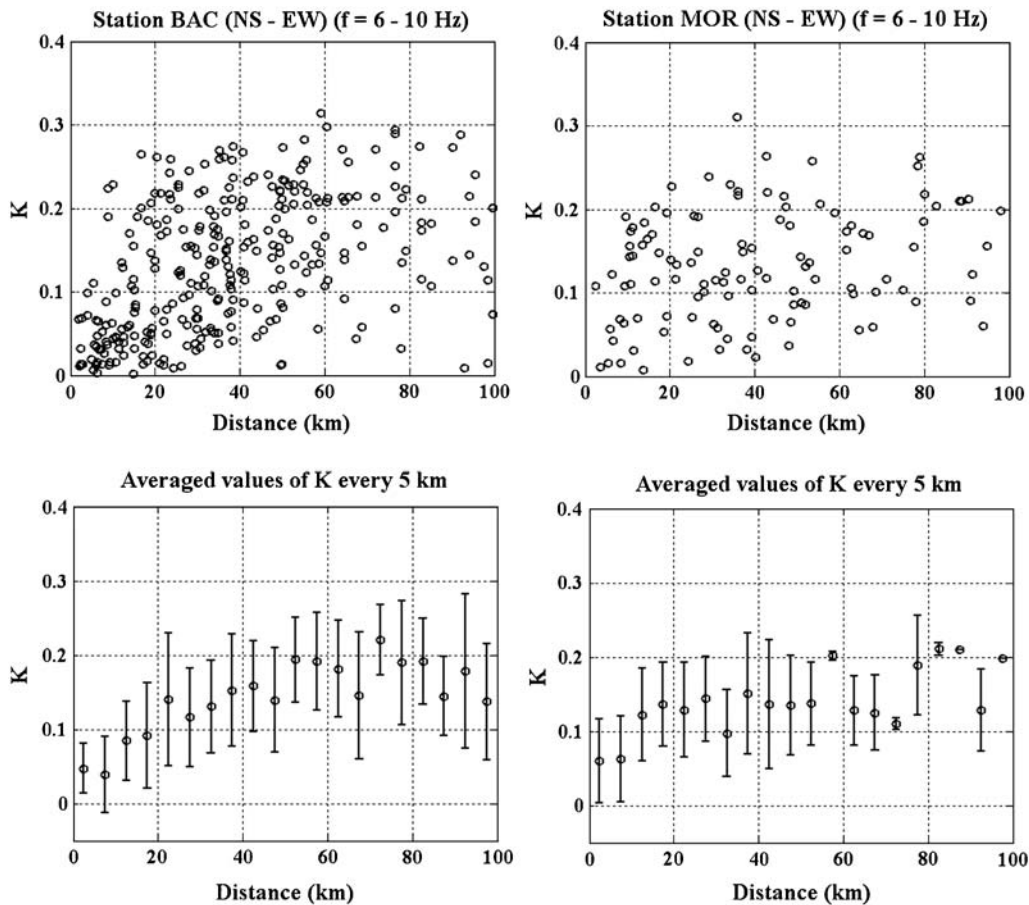


Figure 4. Top frames are κ values estimated at stations BAC (left-hand frame) and MOR (right-hand frame) for distances between 0 and 100 km from all the earthquakes recorded by these stations between 2003 and 2005. The frames at the bottom are the average values of κ calculated at intervals of 5 km.

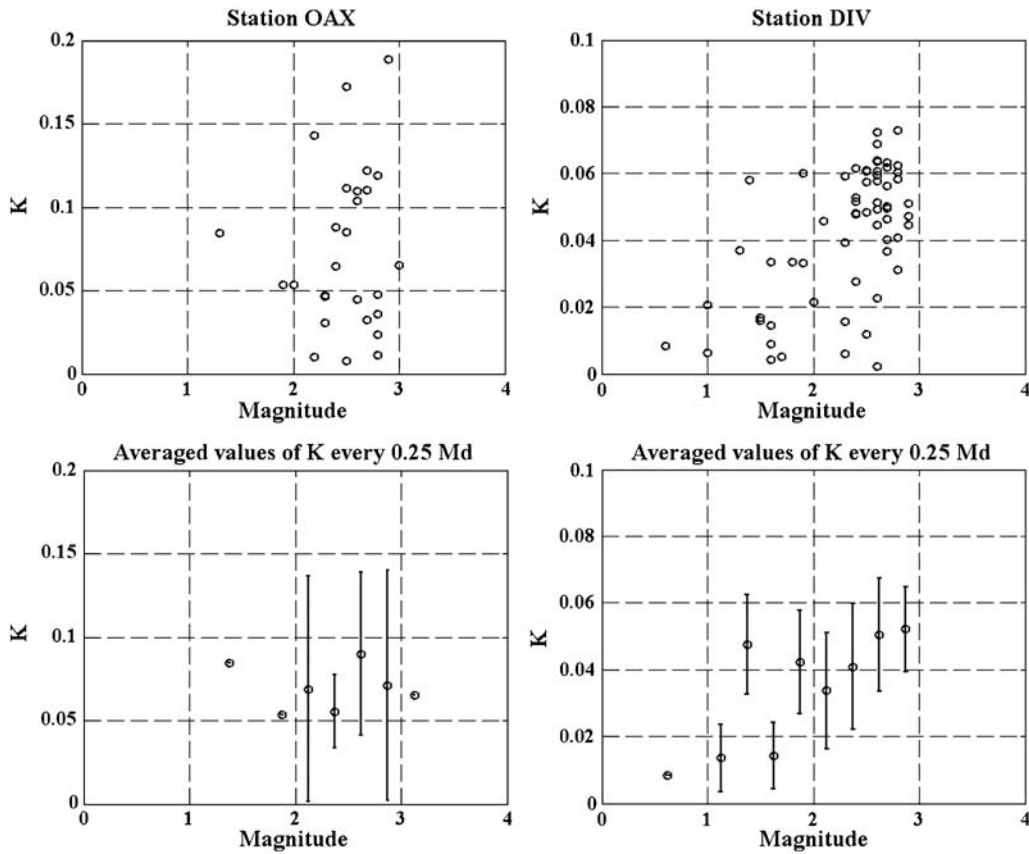


Figure 5. Top frames are κ values estimated at stations OAX (left-hand frame) and DIV (right-hand frame) for magnitudes between 0 and 4. The frames at the bottom are the averaged values of κ calculated at 0.25 magnitude intervals.

The distribution of averaged values of κ versus M_D for all the stations analyzed is grouped by distance intervals every 20 km in Figure 6. We separated the observed values of κ in different distance intervals to minimize the distance dependence of κ and to visualize better the possible dependence of κ on earthquake size. For each distance interval, the dependence of κ with r must be minimal because the length of the source-station path is similar. In the magnitude range $1.4 < M_D < 2.8$, the average κ takes a value close to 0.05 sec for $r < 40$ km and $\kappa \sim 0.10$ sec for r between 40 and 80 km. Then for $M_D > 3.25$, κ increases to 0.15, 0.18, and 0.12 sec for the 20–40, 40–60, and 60–80 km intervals, respectively. These results indicate that in the 1.4–2.8 magnitude interval κ is approximately constant at shorter ($r < 40$ km) and longer ($40 < r < 80$ km) hypocentral distances, and there is not a clear correlation of κ with earthquake size.

Nevertheless, we solved equation (3) considering that κ is a function of both distance and magnitude. Figure 7 shows the resulting surfaces $\kappa(r, M_D)$ estimated inverting equation (5). Notice that these surfaces are scaled according to the value of $\kappa_0(z)$ obtained for each recording site. κ shows a clear dependence with distance and also a specific value of $\kappa_0(z)$ at each station because the surfaces are at different levels of κ . It is also clear in Figure 7 that κ remains basically

constant for different M_D . These results indicate that κ is independent of the earthquake size. Thus, we can use the average values of κ calculated at 5 km intervals to form the system of equations described by equation (5) to find $\kappa(r)$ and $\kappa_0(z)$, after removing from this equation the dependence of κ with magnitude.

The curves in Figure 8, show the function $\kappa(r, z)$ estimated with the nonparametric method described previously. Notice in Figure 8 that while $\kappa(r)$ is the same for all the stations, $\kappa_0(z)$ is unique among each site. We used the estimates of κ from all the stations together to solve equation (2) and to find $\kappa(r)$ and $\kappa_0(z)$.

We also explored if κ_0 correlates with the geological conditions, namely the rock type, of the sites where the stations were installed. For this purpose, the station sites were classified according to their lithology characteristics using geologic maps published by INEGI, as mentioned before. Based on the location of the stations within the superficial geology maps, we classified the stations in three groups: I, stations on extruded acid igneous rocks (Tertiary); II, stations on conglomerates (Tertiary); and III, stations on extruded acid igneous rocks (Cretaceous). Then, the function $\kappa(r, z)$ of equation (2) was estimated again for each of the three groups of stations according to this geologic classification instead of assuming a common $\kappa(r)$ for all individual

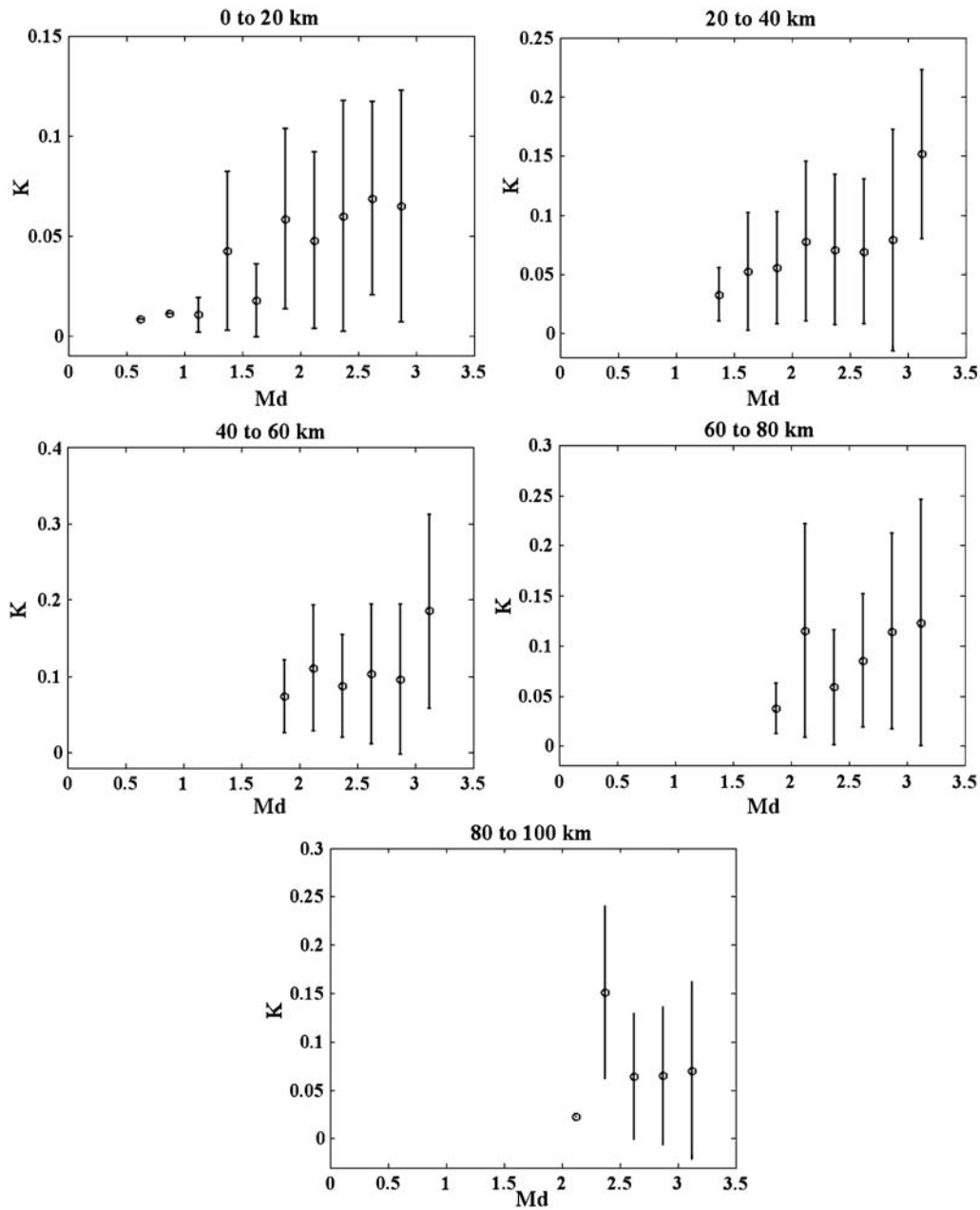


Figure 6. Distribution of average values of κ versus M_D at 0.25 magnitude intervals. Each frame corresponds to a different distance interval, every 20 km.

stations. For each group equation (2) was solved separately. Notice that with this approach $\kappa(r)$ is the same for all stations of the group but may be different between the groups.

Table 1 lists the estimates of κ_0 obtained for the individual stations when solving equation (2) with all the data together and when solving for each group of stations. Table 1 also includes the average values of κ_0 for each group, calculated using all the stations of the group as a whole.

Figure 9 shows the estimated function $\kappa(r, z)$ for the three classified groups. The frames in the left-hand column are the results for three stations selected as an example for each group. The circles are average values of κ obtained for

the station, with its standard deviation, and the solid line is the nonparametric function for the station calculated with all the stations that belong to the group. The dashed lines are the corresponding root mean squares of the estimates. Frames in the right-hand column of Figure 9 show $\kappa(r, z)$ curves calculated for each group.

Under the assumption that stations on sites with the same rock classification have the same value of κ_0 , we recalculated the nonparametric functions. Figure 10 shows $\kappa(r, z)$ estimated for groups of stations with the same geologic classification, using all the stations of the group as if they were at the same site, to calculate the distance dependence function

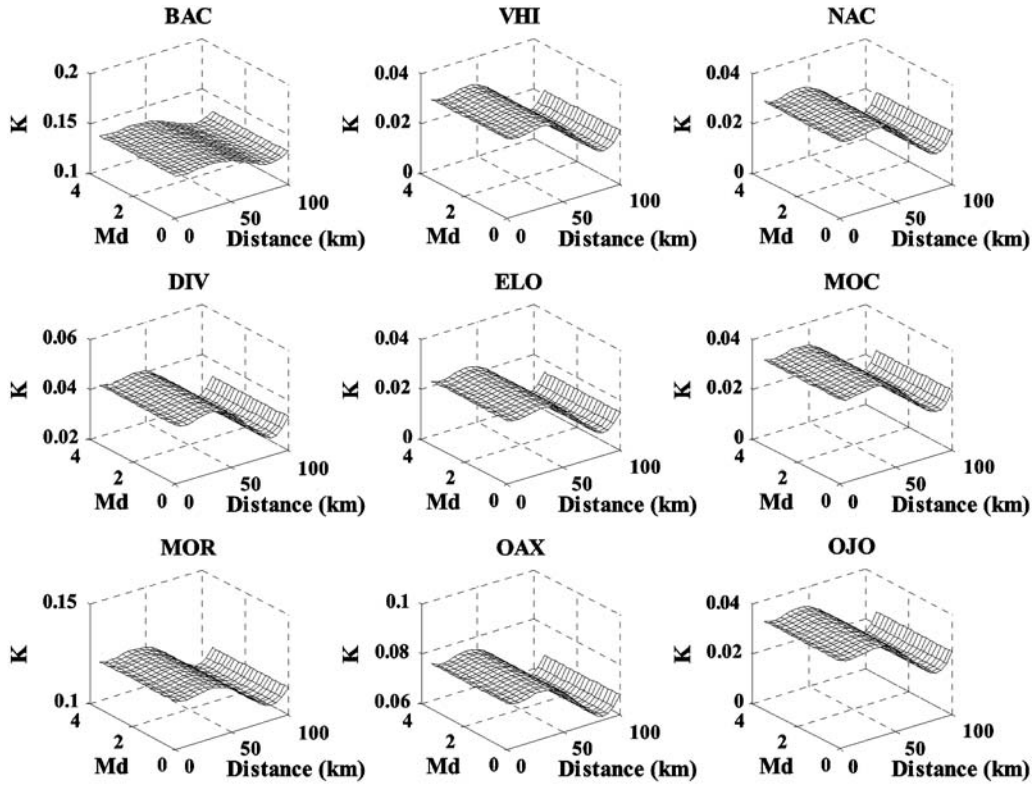


Figure 7. Resulting $\kappa(r, M_D)$ surfaces estimated from equation (5).

$\kappa(r)$ and the average κ_0 value of the group. In this case, we are considering that $\kappa(r)$ is the same for the three groups and that κ_0 is the same for all the stations in the group. Notice in Figure 10 that the resulting function $\kappa(r, z)$ is, in fact, the same for the three groups but is shifted accordingly by the κ_0 value obtained for the group.

Discussion

We determined the high-frequency spectral decay of small earthquakes located in northeastern Sonora using the parameter κ of the Anderson and Hough (1984) model (equation 1). The results of our analysis of κ versus M_D (Figs. 5–7) indicate that κ is basically independent of earthquake size in the magnitude range of the events used ($0.5 < M < 3.5$). Similar results were found by Castro *et al.* (2000) in central Italy for earthquakes with local magnitudes

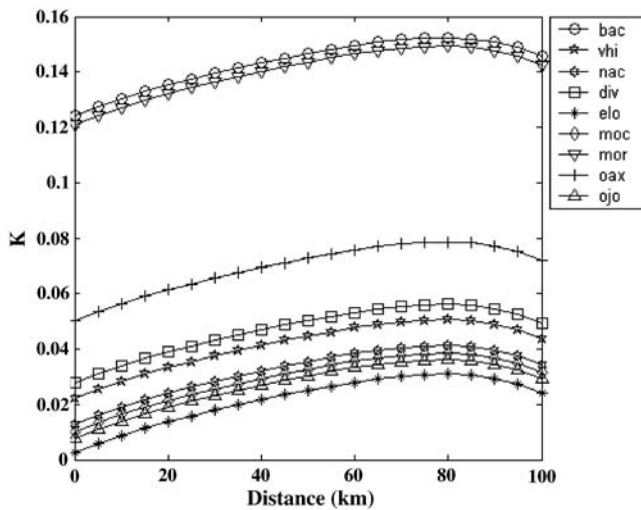


Figure 8. Functions $\kappa(r, z)$ at different sites estimated with the nonparametric method proposed by Anderson and Lei (1994). Note that the dependence of κ with distance is the same for all the stations, but the $\kappa_0(z)$ is unique among the stations.

Table 1

Classification of Recording Stations According to Their Lithology Characteristics and the κ_0 Value Estimated for Each Station and Group

Station	Individual Estimates of κ_0 (With All the Stations)	Group Class*	Individual Estimates of κ_0 (By Groups of Stations)	κ_0 of the Group
OJO	0.0078	I	0.0170	0.0177
ELO	0.0026	I	0.0100	–
NAC	0.0129	I	0.0174	–
OAX	0.0503	II	0.0527	0.0842
MOR	0.1210	II	0.1233	–
VHI	0.0222	II	0.0238	–
MOC	0.0101	II	0.0124	–
BAC	0.1241	II	0.1264	–
DIV	0.0278	III	0.0420	0.0374

*Group I corresponds to stations located on Tertiary acid igneous rocks, group II are stations located on conglomerates (Tertiary), and group III stations are located on Cretaceous acid igneous rocks.

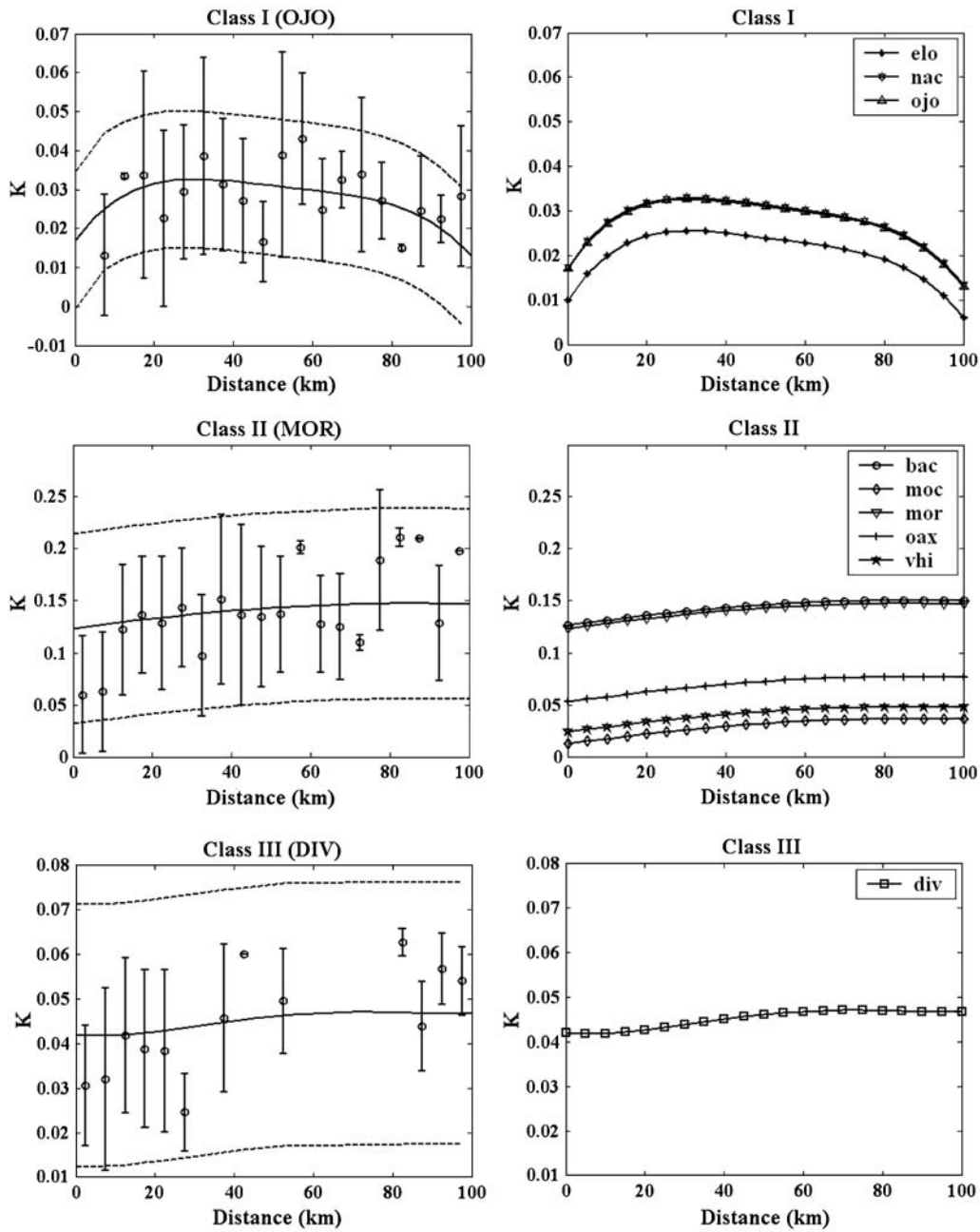


Figure 9. Functions $\kappa(r, z)$ estimated for each group of stations. The frames in the left-hand column are examples of the observed values of κ from one station of each group. The circles are average values of κ of the station selected with its standard deviation. The solid line is $\kappa(r, z)$ obtained for the station selected, and the dashed lines are the corresponding root mean squares. The frames in the right-hand column display the $\kappa(r, z)$ functions calculated for each station of the group.

between 2.1 and 4.1. They found a low correlation between κ and magnitude (see fig. 8 and table 3 of their article). More recently, [Purvance and Anderson \(2003\)](#) studied the relationship between κ and M of earthquakes with different focal mechanisms and observed that a linear correlation exists, with a confidence interval of 99.8% in the frequency band from 10 to 30 Hz, and 88.1% in the frequency of 10–45 Hz. However, the correlation drops to a confidence level of 56.0% in the range of 25–40 Hz. These authors explained this behavior as a source effect because at high frequencies

equation (1) implicitly assumes that the spectrum falls as w^{-2} . In the frequency band from 25 to 40 Hz, the spectral amplitudes appear to be sufficiently distant from the corner frequency and therefore are not affected by source effects, and consequently κ does not seem to correlate with earthquake magnitude. For the other frequency bands used, however, it is possible that the proximity of the corner frequency to 10 Hz, of events with smaller magnitude, may have influenced the obtained κ values. [Purvance and Anderson \(2003\)](#) also found that normal faulting earthquakes and events with

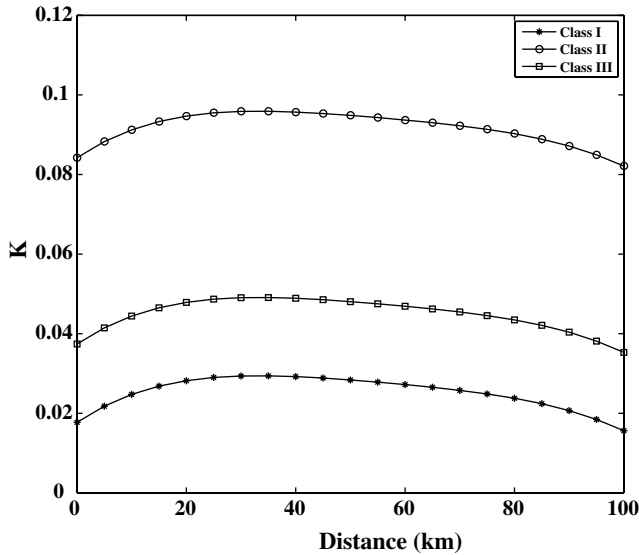


Figure 10. Function $\kappa(r, z)$ estimated for the groups of stations with the same site classification. All the stations of the group are considered as one site to calculate the distance dependence function $\kappa(r)$ and κ_0 is the average value of the group.

reverse focal mechanisms show different spectral characteristics, with normal faulting events having lower values of κ . The average κ of those events (κ_{event}) varies between 0.0012 and 0.007 sec. In our study, we do not know the focal mechanisms of the earthquakes used, but because they are located in the Basin and Range province, we expect many of them to be normal faulting earthquakes. Our equivalent event-average values of κ (Fig. 6) vary between 0.0005 and 0.3135 sec. The minimum values in Figure 6 are consistent with those reported by Purvance and Anderson (2003) for normal faulting earthquakes in Guerrero, México.

We found that for a given distance and recording site the values of κ vary considerably. For instance, at 60 km station BAC shows values of κ that can vary from the minimum to the maximum value by a factor of up to 6 times (see Fig. 4). Because the source-station azimuths of the spectral records are not constant, we interpret the observed variability of κ as the result of lateral heterogeneity of the propagating media. To reduce this variability, we averaged κ within 5 km intervals between 0 and 100 km and calculated nonparametric functions that describe the distance dependence of κ and that give an estimate of the attenuation near the surface. These empirically determined curves (Fig. 8) give expected values of κ that increase with distance up to 80 km; then the κ functions become approximately constant between 80 and 85 km and tend to decrease at higher distances. Because at short distances the ray paths are shallow, the nonparametric functions obtained indicate higher S -wave attenuation at shallow depths and lower attenuation for deeper paths. These results are consistent with previous estimates of Q reported by Castro *et al.* (2009). They found in the same region that the quality factor Q is higher in the lower crust, indicating lower attenuation compared with that in the upper crust.

We analyzed also the effect of surface geology on the distance dependence of κ by classifying the estimates of κ according to the geologic characteristics at the recording sites. We found that the empirical curves (Fig. 9) that describe the behavior of the spectral decay parameter κ with distance are different for the three site classifications analyzed in the region. This difference may be due to stations of each class sampling different crustal volumes with specific geological and tectonic characteristics. The $\kappa(r)$ functions obtained with stations in class I (OJO, NAC, and ELO) increase with distance up to 20 km, remain approximately constant up to 35 km, and then begin to decline slowly, decreasing sharply at 80 km. The nonparametric curves for the class II group of stations give values of κ that increase with distance for the whole distance range considered (0–100 km). For the class III group, κ increases up to 70 km and then the curve flattens.

The estimates of near-surface attenuation (κ_0) show that stations on extruded acid igneous rocks of the Tertiary have the smallest values of near-surface attenuation. Station DIV, situated to the south of the fault zone (see Fig. 1) and located on extruded acid igneous rocks but geologically older than the stations of group I, has a slightly bigger κ_0 . Stations in the class II group have κ_0 values that vary from 0.0101 sec at station MOC to 0.1241 sec, the biggest value of all stations, at BAC. In the class II group the reported conglomerates correspond to sedimentary rocks with high attenuation. The variations of κ_0 obtained for this group may be related with the specific composition of the conglomerates and with the degree of consolidation. The conglomerates predominate in the region and may have an important influence in the behavior of κ with distance. When we assume that all stations in a given group have the same near-surface attenuation (Fig. 10), we still observe a similar behavior for the near-surface attenuation, κ_0 taking values of 0.0177 sec for class I, 0.0374 sec for class III, and the biggest value of 0.0842 sec for class II (Table 1).

The previous values of κ_0 are similar to results obtained in other regions. For instance, Castro *et al.* (1996) found in the region of Friuli, Italy, that the spectral decay parameter κ_0 is smaller for stations located on hard rocks compared with stations located on sites with less competent geology. They estimated an average κ_0 over the network of 0.03 sec. Similar results were also previously reported by Anderson and Hough (1984) for California. We obtained, coincidentally, an average κ_0 of 0.04 sec for the stations of RESNES. Hough, *et al.* (1988) estimated κ from the Anza array in southern California and obtained smaller κ_0 values that range from 0.0003 to 0.0181 sec.

Regarding the observed variability of κ with distance, Castro *et al.* (2000) also reported in the region of Umbria-Marche, Italy, great variability in the estimates of κ for similar source-station paths. They interpreted this observation as possibly due to the degree of fracturing along the propagation path.

Conclusions

The empirical curves obtained describe the distance and site dependence of the spectral decay parameter κ and indicate that the near-surface attenuation is different for the three site classifications analyzed in the region of Sonora. Our results (Figs. 5–7) indicate that κ is independent of earthquake size within the magnitude range ($M < 3.5$) of the events analyzed. The nonparametric curves also indicate that S waves attenuate more at short distances ($r < 80$ km) because κ tends to increase in this distance range. This result is in agreement with a previous study (Castro *et al.*, 2009) that reports lower values of Q in the upper crust compared with Q in the lower crust.

We conclude that κ_0 depends not only on the rock type but also on the degree of fracturing and erosion of the rocks. We found an average value of κ_0 of 0.04 sec for northeastern Sonora that is similar to values reported in other regions.

Data and Resources

The seismograms used in this article were recorded by permanent stations of the RESNES seismic array. Data from this network can be requested from the second author of this article. Some plots were made using the Generic Mapping Tools (www.soest.hawaii.edu/gmt) [last accessed September 2009]; Wessel and Smith, 2009).

Acknowledgments

The installation and operation of the Seismic Network of Northeastern Sonora (RESNES) has been possible thanks to the financial support of the Mexican National Council for Science and Technology (CONACYT) by means of the projects G33102-T and 59216. We are grateful for technical support provided by Luis Inzunza, Antonio Mendoza, and Arturo Perez Vertti. We are also thankful for the participation of Cesar Jacques and Alejandro Hurtado from the Instituto de Geología de la Universidad Nacional Autónoma de México (UNAM). Max Suter and Oscar Romero participated during the initial part of the project, and José M. Romo helped us during the elaboration of the computer code used. This article was completed while one of the authors (RRC) was a UC MEXUS-CONACYT Visiting Scholar at the University of California, San Diego, IGPP-SIO. We are grateful for the comments of the two anonymous reviewers and associate editor Arthur McGarr.

References

Anderson, J. G. (1991). A preliminary descriptive model for the distance dependence of the spectral decay parameter in southern California, *Bull. Seismol. Soc. Am.* **81**, 2186–2193.

Anderson, J. G., and S. E. Hough (1984). A model for the shape of the Fourier amplitude spectrum of acceleration at high frequencies, *Bull. Seismol. Soc. Am.* **74**, 1969–1993.

Anderson, J. G., and Y. Lei (1994). Nonparametric description of peak acceleration as a function of magnitude, distance, and site in Guerrero, Mexico, *Bull. Seismol. Soc. Am.* **84**, 1003–1017.

Beresnev, I. A., and G. M. Atkinson (1997). Modeling finite-fault radiation from the ω^p spectrum, *Bull. Seismol. Soc. Am.* **87**, 67–84.

Bindi, D., R. R. Castro, G. Franceschina, L. Luzi, and F. Pacor (2004). The 1997–1998 Umbria-Marche sequence (central Italy): Source, path and site effects estimated from strong motion data recorded in the epicentral area, *J. Geophys. Res.* **109**, B04312.

Castro, R. R., C. Condori, O. Romero, C. Jacques, and M. Suter (2008). Seismic attenuation in northeastern Sonora, Mexico, *Bull. Seismol. Soc. Am.* **98**, 722–732.

Castro, R. R., C. I. Huerta, O. Romero, C. Jacques, A. Hurtado, and A. I. Fernández (2009). Body-wave attenuation near the rupture of the 1887 Sonora, Mexico, earthquake (M_w 7.5) *Geofis. Int.* **48**, 297–304.

Castro, R. R., F. Pacor, A. Sala, and C. Petrangaro (1996). S wave attenuation and site effects in the region of Friuli, Italy, *J. Geoph. Res.* **101**, no. B10, 22,355–22,369.

Castro, R. R., O. M. Romero, and M. Suter (2002). Red sísmica para el monitoreo de la sismicidad del sistema de fallas normales del noreste de Sonora, *Geos.* **22**, 379 (in Spanish).

Castro, R. R., A. Rovelli, M. Cocco, M. Di Bona, and F. Pacor (2001). Stochastic simulation of strong-motion records from the 26 September 1997 (M_w 6), Umbria-Marche (central Italy) earthquake, *Bull. Seismol. Soc. Am.* **91**, 27–39.

Castro, R. R., L. Trojani, G. Monachesi, M. Mucciarelli, and M. Cattaneo (2000). The spectral decay parameter κ in the region of Umbria-Marche, Italy, *J. Geoph. Res.* **105**, 23,811–23,823.

Condori, S. C. (2006). Estudio de atenuación sísmica de la región noreste de Sonora, *Master's Thesis*, CICESE.

González, J. J., and R. García (1986). Escala de magnitud-coda para estaciones sismográficas en el norte de Baja California, *Resumen Extenso en Memorias de la Reunión 1986 de la Unión Mexicana, A.C.*, 399–406.

Hough, S. E., J. G. Anderson, J. Brune, F. Vernon III, J. Berger, J. Fletcher, L. Haar, T. Hanks, and L. Baker (1988). Attenuation near Anza, California, *Bull. Seismol. Soc. Am.* **78**, 672–691.

Mexican National Institute of Statistics, Geography and Information (INEGI) (2006). Carta geológica del Estado de Sonora, scale 1:1,000,000.

Papageorgiou, A. S., and K. Aki (1983). A specific barrier model for the quantitative description of inhomogeneous faulting and prediction of strong motion. I. Description of model, *Bull. Seismol. Soc. Am.* **73**, 693–722.

Petukhin, A., and K. Irikura (2000). A method for the separation of the source and site effects and the apparent Q structure from strong-motion data, *Geophys. Res. Lett.* **27**, 3429–3432.

Purvance, M. D., and J. G. Anderson (2003). A comprehensive study of the observed spectral decay in strong-motion accelerations recorded in Guerrero, Mexico, *Bull. Seismol. Soc. Am.* **93**, 600–611.

Rovelli, A., O. Bonamassa, M. Cocco, M. Di Bona, and S. Mazza (1988). Scaling laws and spectral parameters of the ground motions in active extensional areas in Italy, *Bull. Seismol. Soc. Am.* **78**, 530–560.

Suter, M., and J. Contreras (2002). Active tectonics of northeastern Sonora, Mexico (southern Basin and Range province) and the 3 May 1887 M_w 7.4 earthquake, *Bull. Seismol. Soc. Am.* **92**, 581–589.

Tsai, C.-C. P., and K.-C. Chen (2000). A model for the high-cut process of strong motion acceleration in terms of distance, magnitude, and site condition: An example from the SMART1 array, Lotung, Taiwan, *Bull. Seismol. Soc. Am.* **90**, 1535–1542.

Wessel, P., and W. H. F. Smith (2009). *The Generic Mapping Tools (GMT) version 4.5.0 technical Reference & Cookbook*, SOEST/NOAA.

Centro de Investigación Científica y de Educación Superior de Ensenada (CICESE)
División Ciencias de la Tierra
Departamento de Sismología
km 107 Carretera Tijuana-Ensenada
22860 Ensenada, Baja California, México
raul@cicese.mx